TENSOR-GUIDED INTERPOLATION FOR OFF-GRID POWER SPECTRUM MAP CONSTRUCTION

Hao Sun[1,2], *Junting Chen*[1,2] *and Yuan Luo*[1,3]

[1]School of Science and Engineering and [2]Future Network of Intelligence Institute,
The Chinese University of Hong Kong, Shenzhen, China
[3]Shenzhen Institute of Artificial Intelligence and Robotics for Society, Shenzhen, China

ABSTRACT

This paper addresses the off-grid tensor-guided interpolation problem, aiming to reconstruct a 3D power spectrum map from sparse observations. A segmented polynomial model is employed to handle off-grid measurements, while a nuclear norm regularization is incorporated to account for the inherent low-rank characteristics of signals. An alternating regression and singular value thresholding algorithm is developed to solve the proposed method. The numerical results demonstrate the superiority of the proposed method, showcasing a remarkable improvement of over 10% in power spectrum map reconstruction accuracy when the sampling rate exceeds 6%, as compared to state-of-the-art approaches.

***Index Terms*—** Tensor-guided, interpolation, off-grid, alternating minimization, power spectrum map.

1. INTRODUCTION

Power spectrum map enables many applications in wireless signal processing, including localization [1–3], wireless power transfer [4], resource management [5], etc. Particularly, the multidimensional nature of wireless signals, e.g., the signals detected from different frequency bands, enables the opportunities for tensor structure to be applied in the processing of power spectrum map. However, the signals measured from real world are not necessarily on-grid and exist sparse nature. Exploiting the correlation across the spectral domain of signals continues to pose a challenge. To enhance the efficiency and accuracy for power spectrum map construction, a tensor-guided interpolation method is thus developed in this paper.

Traditional interpolation methods including Kriging [6], kernel based method [7, 8], and sparse representation methods such as dictionary learning [9, 10], matrix completion [1, 11, 12] mainly focus on the 2D power spectrum map construction. These methods construct the multidimensional power spectrum map by independently reconstructing each slice, resulting in high computational complexity. Deep learning-based approaches [13, 14] have gained prominence with the advent of big data. However, these methods are computationally intensive and can pose challenges in terms of interpretability.

Tensor completion [5, 15] and tensor decomposition [16, 17] methods have garnered attention for their potential in reconstructing the multi-dimensional power spectrum map. Most existing tensor-based methods require on-grid sampling, i.e., the measurements locate on the grid center. However, this requirement is rarely met in practice. When the grid size is large, a significant discretization error occurs, which can degrade the performance of tensor completion. Conversely, when the grid size is small, meaning there are more grid points for finer spatial resolution, an identifiability issue can arise in tensor completion. An interpolation method is adapted in [17] to deal with the off-grid issue. However, the interpolation and tensor decomposition work separately in an open-loop form. A poor interpolation may affect the tensor completion step.

This paper attempts to address the identifiability issue in tensor completion for power spectrum map construction from sparse and off-grid measurements. A segmented polynomial model is adopted for interpolating the power spectrum map, and a tensor-guided interpolation problem exploiting the block term tensor decomposition (BTD) structure is formulated. The proposed formulation exploits two properties from the BTD model: First, there is spatial correlation of propagation over different frequency bands, and second, the power

Junting Chen is the corresponding author. The work was supported in part by the National Science Foundation of China under Grant No. 62102343, by the Basic Research Project No. HZQB-KCZYZ-2021067 of Hetao Shenzhen-HK S&T Cooperation Zone, by the Shenzhen Science and Technology Program under Grant No. JCYJ20220530143804010, No. KQTD20200909114730003, No. JCYJ20220818103006012, and No. JCYJ20230807114300001, by Guangdong Research Projects No. 2019QN01X895, No. 2017ZT07X152, and No. 2019CX01X104, by the Shenzhen Outstanding Talents Training Fund 202002, by the Guangdong Provincial Key Laboratory of Future Networks of Intelligence (Grant No. 2022B1212010001), by the National Key R&D Program of China with grant No. 2018YFB1800800, by the Key Area R&D Program of Guangdong Province with grant No. 2018B030338001, Shenzhen Key Lab of Crowd Intelligence Empowered Low-Carbon Energy Network (No. ZDSYS20220606100601002), and the Shenzhen Institute of Artificial Intelligence and Robotics for Society.

maps have low-rank structure. We develop an alternating regression and singular value thresholding algorithm to solve the tensor-guided interpolation problem. We observe from the numerical experiments that more than 10% improvement in the reconstruction accuracy is achieved compared to the state-of-the-art approaches.

2. SYSTEM MODEL

2.1. Signal Model

Consider that a bounded area $\mathcal{D} \subseteq \mathbb{R}^2$ contains R signal sources. The signals occupying K frequency bands are detected by M sensors at known locations $\boldsymbol{z}_m \in \mathcal{D}$, $m = 1, 2, \dots, M$. Denote $\boldsymbol{s}_r \in \mathcal{D}$ as the location of the rth source. Then, the signal power from the rth signal source measured at the kth frequency band and location $\boldsymbol{z}$ is modeled as [16, 18]

$$\rho_k^{(r)}(\boldsymbol{z}) = \left(g_r(d(\boldsymbol{s}_r, \boldsymbol{z})) + \zeta_r(\boldsymbol{z}) + \eta_{r,k}(\boldsymbol{z})\right)\phi_k^{(r)} \quad (1)$$

where $g_r(d(\boldsymbol{s}_r, \boldsymbol{z}))$ describes the path gain of the rth source at distance d, the function $d(\boldsymbol{s}, \boldsymbol{z}) = \|\boldsymbol{s} - \boldsymbol{z}\|_2$ describes the distance between a source at $\boldsymbol{s}$ and a sensor at $\boldsymbol{z}$, $\zeta_r(\boldsymbol{z})$ captures the shadowing of the signal from the rth source, $\eta_{r,k}(\boldsymbol{z})$ is a zero mean Gaussian random variable to model the fluctuation due to the frequency-selective fading, and $\phi_k^{(r)}$ describes the power allocation of the rth source at the kth frequency band.

The aggregated power at the kth frequency band from all the R sources measured by some sensor located at $\boldsymbol{z}_m$ is denoted as $\gamma_m^{(k)} = \sum_{r=1}^{R} \rho_k^{(r)}(\boldsymbol{z}_m) + \epsilon, \forall k \in \Omega_m$, where $\epsilon \sim \mathcal{N}(0, \sigma^2)$ is to model the measurement noise, and $\Omega_m \subseteq \{1, 2, \dots, K\}$ contains the set of frequency bands that are measured by the mth sensor.

Our goal is to reconstruct the propagation field

$$\rho^{(r)}(\boldsymbol{z}) = g_r(d(\boldsymbol{s}_r, \boldsymbol{z})) + \zeta_r(\boldsymbol{z}) \quad (2)$$

i.e., the first two terms in (1), and the power spectrum $\phi_k^{(r)}$, $k = 1, 2, \dots, K$, for each source r. As a result, based on the propagation model (1), the measurement model can be derived as

$$\gamma_m^{(k)} = \sum_{r=1}^{R} \rho^{(r)}(\boldsymbol{z}_m)\phi_k^{(r)} + \tilde{\epsilon} \quad (3)$$

where $\tilde{\epsilon} = \eta_{r,k}(\boldsymbol{z})\phi_k^{(r)} + \epsilon$ is a zero mean random variable that combines the randomness due to the frequency-selective small-scale fading $\eta_{r,k}(\boldsymbol{z})\phi_k^{(r)}$ and the measurement noise ϵ.

2.2. Tensor Model

Consider to discretize the target area $\mathcal{D}$ into N_1 rows and N_2 columns that results in $N_1 \times N_2$ grid cells. Let $\boldsymbol{c}_{ij} \in \mathcal{D}$ be the center location of the (i, j)th grid cell. Let $\boldsymbol{S}_r \in \mathbb{R}^{N_1 \times N_2}$ be a discretized form of the propagation field for the rth source, where the (i, j)th entry is given by $[\boldsymbol{S}_r]_{(i,j)} = \rho^{(r)}(\boldsymbol{c}_{ij})$. It has been widely discussed in the literature that for many common propagation scenarios, the matrix $\boldsymbol{S}_r$ exists low-rank property [12, 16].

Let $\boldsymbol{\mathcal{H}} \in \mathbb{R}^{N_1 \times N_2 \times K}$ be a tensor representation of the *target* power spectrum map to be constructed. Based on (1), we use $[\boldsymbol{\mathcal{H}}]_{(i,j,k)} = \sum_{r=1}^{R} \rho^{(r)}(\boldsymbol{c}_{ij})\phi_k^{(r)}$ to represent the aggregated power of the kth frequency band measured at location $\boldsymbol{c}_{ij}$ exempted from the small-scale fading component $\eta_{r,k}(\boldsymbol{z})\phi_k^{(r)}$. Denote $\boldsymbol{\phi}^{(r)} = [\phi_1^{(r)}, ..., \phi_K^{(r)}]^{\mathrm{T}}$ as the power spectrum from the rth source. As a result, the tensor $\boldsymbol{\mathcal{H}}$ has the following BTD structure

$$\boldsymbol{\mathcal{H}} = \sum_{r=1}^{R} \boldsymbol{S}_r \circ \boldsymbol{\phi}^{(r)} \quad (4)$$

where '$\circ$' represents outer product.

Conventional tensor-based power spectrum map construction approaches can complete the tensor $\boldsymbol{\mathcal{H}}$ in (4) from the measurement $\gamma_m^{(k)}$ in (3), but they require the measurement $\gamma_m^{(k)}$ to be taken at the center of the grid cell [5, 15]. However, when the grid cells are too large, corresponding to small N_1 and N_2, it is hard to guarantee that the sensor at $\boldsymbol{z}_m$ is placed at the corresponding grid center $\boldsymbol{c}_{ij}$, resulting in possibly large discretization error. When the grid cells are small, corresponding to large N_1 and N_2, there might be an identifiability issue as the dimension of the tensor is large.

Recent attempts [17, 18] consider to first estimate $[\boldsymbol{\mathcal{H}}]_{(i,j,k)}$ using interpolation methods based on the off-grid measurements, and then, employ tensor completion based on the BTD model (3) to improve the spectrum map construction. However, these methods are open-loop method, where the property that $\boldsymbol{S}_r$ are low-rank matrices is not exploited in the interpolation step; and as a result, a poor interpolation may affect the performance in the tensor completion step.

3. TENSOR-GUIDED INTERPOLATION

In this section, we propose a closed-loop method for tensor-guided interpolation, such that the BTD structure of the tensor model and low-rank property of the tensor components are both exploited for interpolation.

3.1. The Tensor-guided Interpolation Problem

Based on the BTD model in (4), we consider to construct a model $f^{(r)}(\boldsymbol{z})$ for the component $\boldsymbol{S}_r$ such that $f^{(r)}(\boldsymbol{z})$ benefit from the low-rank structure of $\boldsymbol{S}_r$, in addition, we also need to estimate the power spectrum $\boldsymbol{\phi}^{(r)}$ to fit the measurement data $\gamma_m^{(k)}$.

Here, we adopt a segmented polynomial model for $f^{(r)}(\boldsymbol{z})$. Specifically, we construct R polynomial models $f_{ij}^{(r)}(\boldsymbol{z})$, $r = 1, 2, \dots, R$, for each grid cell (i, j) centered at c_{ij}. Without loss of generality (w.l.o.g.), a second order Taylor polynomial model is given as follows

$$f_{ij}^{(r)}(\boldsymbol{z}) = \alpha_{ij}^{(r)} + \boldsymbol{\beta}_{ij}^{(r)\mathrm{T}}(\boldsymbol{z}-\boldsymbol{c}_{ij}) + (\boldsymbol{z}-\boldsymbol{c}_{ij})^{\mathrm{T}}\boldsymbol{B}_{ij}^{(r)}(\boldsymbol{z}-\boldsymbol{c}_{ij}) \quad (5)$$

where $\boldsymbol{\theta}_{ij}^{(r)} = [\alpha_{ij}^{(r)}, (\boldsymbol{\beta}_{ij}^{(r)})^{\mathrm{T}}, (\mathrm{vec}(\boldsymbol{B}_{ij}^{(r)}))^{\mathrm{T}}]^{\mathrm{T}} \in \mathbb{R}^7$ is a collection of model parameters for the propagation field of the rth source and grid cell (i,j), vec$(\boldsymbol{A})$ represents the vectorization of $\boldsymbol{A}$.

To estimate the parameters $\boldsymbol{\theta}_{ij}^{(r)}$ in $f_{ij}^{(r)}(\boldsymbol{z})$, we then formulate a least-squares local polynomial regression problem based on the measurement model (3) as follows:

$$\underset{\{\boldsymbol{\theta}_{ij}^{(r)}\}}{\text{minimize}} \sum_{m=1}^{M}\sum_{k\in\Omega_m}\left(\gamma_m^{(k)} - \sum_{r=1}^{R} f_{ij}^{(r)}(\boldsymbol{z}_m)\phi_k^{(r)}\right)^2 F_{ij}(\boldsymbol{z}_m) \quad (6)$$

where $F_{ij}(\boldsymbol{z}) \triangleq F((\boldsymbol{z}-\boldsymbol{c}_{ij})/b)$ is a kernel function with a parameter b to weight the importance of the measurements. A possible choice can be the Epanechnikov kernel $F(\boldsymbol{u}) = \max\{0, \frac{3}{4}(1-||\boldsymbol{u}||^2)\}$ [19].

A global model $f^{(r)}(\boldsymbol{z})$ can be constructed based on a number of local models $f_{ij}^{(r)}(\boldsymbol{z})$ on selected cells $(i,j)\in\Omega$. As a result, the cost function for the global model $f^{(r)}(\boldsymbol{z})$ can be written as

$$l(f) = \sum_{(i,j)\in\Omega} l_{ij}(\boldsymbol{\theta}_{ij}, \boldsymbol{\Phi})$$

where $\boldsymbol{\theta}_{ij} = [\boldsymbol{\theta}_{ij}^{(1)} \cdots \boldsymbol{\theta}_{ij}^{(R)}] \in \mathbb{R}^{7\times R}$, $\boldsymbol{\Phi} = \{\phi_k^{(r)}\}$, and $l_{ij}(\cdot)$ is the cost function in (6).

The BTD suggests that when one samples $f^{(r)}(\boldsymbol{z})$ over $N_1 \times N_2$ grid points $\{\boldsymbol{c}_{ij}\}$, the resulting matrix may be low-rank. We thus propose the following tensor-guided interpolation formulation to impose the low-rankness for the global model f:

$$\underset{\{\boldsymbol{\theta}_{ij},\boldsymbol{\Phi}_{ij}\},\{\boldsymbol{S}_r\}}{\text{minimize}} l(f) + \frac{\nu}{2}\sum_{(i,j)}\sum_{r=1}^{R}(f_{ij}^{(r)}(\boldsymbol{c}_{ij}) - [\boldsymbol{S}_r]_{(i,j)})^2 + \mu\sum_{r=1}^{R}\|\boldsymbol{S}_r\|_* \quad (7)$$

where $\|\cdot\|_*$ represents the nuclear norm. As a result, the regression model f not only needs to fit the measurement data $\gamma_m^{(k)}$ via minimizing the cost $l_{ij}(\cdot)$ in (6) but is also penalized by the rank of $\boldsymbol{S}_r$ via the second and the third terms in (7).

3.2. Alternating regression and singular value thresholding

We propose to employ an alternating regression and singular value thresholding method to handle the tensor-guided interpolation formulation (7). For the convenience of expression, we write (7) into the matrix form as follows:

$$\underset{\{\boldsymbol{\theta}_{ij}\},\boldsymbol{\Phi},\{\boldsymbol{S}_r\}}{\text{minimize}} \sum_{(i,j)}\|\boldsymbol{W}_{ij}(\mathrm{vec}(\boldsymbol{\Gamma}) - \tilde{\boldsymbol{D}}_{ij}\boldsymbol{\theta}_{ij})\|_2^2 + \nu\times \sum_{(i,j)}\sum_{r=1}^{R}(\boldsymbol{e}_r^{\mathrm{T}}\boldsymbol{\theta}_{ij} - [\boldsymbol{S}_r]_{(i,j)})^2 + \mu\sum_{r=1}^{R}\|\boldsymbol{S}_r\|_* \quad (8)$$

where $\boldsymbol{x}_m = [1, (\boldsymbol{z}_m - \boldsymbol{c}_{ij})^{\mathrm{T}}, \mathrm{vec}((\boldsymbol{z}_m-\boldsymbol{c}_{ij})(\boldsymbol{z}_m-\boldsymbol{c}_{ij})^{\mathrm{T}})^{\mathrm{T}}] \in \mathbb{R}^{1\times 7}$, $\boldsymbol{D}_{m,k} = [\boldsymbol{x}_m\phi_k^{(1)}, \cdots, \boldsymbol{x}_m\phi_k^{(R)}] \in \mathbb{R}^{1\times 7R}$, $\boldsymbol{D}_k = [\boldsymbol{D}_{1,k}^{\mathrm{T}}, \boldsymbol{D}_{2,k}^{\mathrm{T}}, ..., \boldsymbol{D}_{M,k}^{\mathrm{T}}]^{\mathrm{T}} \in \mathbb{R}^{M\times 7R}$, $\tilde{\boldsymbol{D}}_{ij} = [\boldsymbol{D}_1^{\mathrm{T}}, \boldsymbol{D}_2^{\mathrm{T}}, \cdots, \boldsymbol{D}_K^{\mathrm{T}}]^{\mathrm{T}} \in \mathbb{R}^{MK\times 7R}$, $\boldsymbol{w}_{ij} = [w_1(\boldsymbol{c}_{ij}), w_2(\boldsymbol{c}_{ij}), \cdots, w_M(\boldsymbol{c}_{ij})]$, $w_m(\boldsymbol{c}_{ij}) = \sqrt{F_{ij}(\boldsymbol{z}_m)}$, $\boldsymbol{W}_{ij} = \mathrm{diag}(\boldsymbol{1}^{\mathrm{T}}\otimes\boldsymbol{w}_{ij}) \in \mathbb{R}^{MK\times MK}$, '$\otimes$' is Kronecker product, $\boldsymbol{1}\in\mathbb{R}^K$ is all 1's vector, diag$(\boldsymbol{x})$ is a diagonal matrix whose diagonal elements are the entries of vector $\boldsymbol{x}$, $\boldsymbol{\Gamma}(m,k) = \gamma_m^{(k)} \in \mathbb{R}^{M\times K}$, and $\boldsymbol{e}_r$ is a unit vector with the $(7\times(r-1)+1)$th entry equals 1.

To solve (8), we can update $\phi_k^{(r)}$ and $\boldsymbol{\theta}_{ij}$ through regression and update $\boldsymbol{S}_r$ using singular value thresholding. Based on the updated values of $\boldsymbol{S}_r$ and $\phi_k^{(r)}$, we can solve the following weighted least-squares problem for obtaining the value of parameter $\boldsymbol{\theta}_{ij}$.

$$\underset{\{\boldsymbol{\theta}_{ij}\}}{\text{minimize}} \sum_{(i,j)}\|\boldsymbol{W}_{ij}(\mathrm{vec}(\boldsymbol{\Gamma}) - \tilde{\boldsymbol{D}}_{ij}\boldsymbol{\theta}_{ij})\|_2^2 + \nu\sum_{(i,j)}\sum_{r=1}^{R}(\boldsymbol{e}_r^{\mathrm{T}}\boldsymbol{\theta}_{ij} - [\boldsymbol{S}_r]_{(i,j)})^2 \quad (9)$$

Note that the problem (9) is unconstrained convex problem. Hence, we can find the solution by setting the first order derivative of (9) to zero and get:

$\hat{\boldsymbol{\theta}}_{ij} = (\tilde{\boldsymbol{D}}_{ij}^{\mathrm{T}}\boldsymbol{W}_{ij}\tilde{\boldsymbol{D}}_{ij} + \nu\sum_{r=1}^{R}\boldsymbol{e}_r\boldsymbol{e}_r^{\mathrm{T}})^{-1}(\tilde{\boldsymbol{D}}_{ij}^{\mathrm{T}}\boldsymbol{W}_{ij}\mathrm{vec}(\boldsymbol{\Gamma}) + \nu\sum_{r=1}^{R}\boldsymbol{e}_r[\boldsymbol{S}_r]_{(i,j)})$.

Similarly, we can update $\phi_k^{(r)}$ by weighted least-squares problem based on the updated values of $\boldsymbol{S}_r$ and $\boldsymbol{\theta}_{ij}$ as follows:

$$\underset{\{\phi_k^{(r)}\}}{\text{minimize}} \sum_{(i,j)}\sum_{m=1}^{M}\sum_{k=1}^{K}\left(\gamma_m^{(k)} - \boldsymbol{f}_{ij}\boldsymbol{\phi}_k\right)^2 F_{ij}(\boldsymbol{z}_m) \quad (10)$$

where $\boldsymbol{f}_{ij} = [f_{ij}^{(1)}, \cdots, f_{ij}^{(R)}]$ and $\boldsymbol{\phi}_k = [\phi_k^{(1)}, ..., \phi_k^{(R)}]^{\mathrm{T}}$. A closed-form solution is obtained:

$\hat{\boldsymbol{\phi}}_k = (\sum_{(i,j)}\sum_{m=1}^{M}\boldsymbol{f}_{ij}^{\mathrm{T}}\boldsymbol{f}_{ij}F_{ij}(\boldsymbol{z}_m))^{-1}\sum_{(i,j)}\sum_{m=1}^{M}\gamma_m^{(k)}\boldsymbol{f}_{ij}^{\mathrm{T}}F_{ij}(\boldsymbol{z}_m)$.

With the $\boldsymbol{\theta}_{ij}$ and $\phi_k^{(r)}$ updated by solving (9) and (10), we can update $\boldsymbol{S}_r$ through solving the following low-rank matrix completion problem:

$$\underset{\{\boldsymbol{S}_r\}}{\text{minimize}} \sum_{(i,j)}\sum_{r=1}^{R}(\boldsymbol{e}_r^{\mathrm{T}}\boldsymbol{\theta}_{ij} - [\boldsymbol{S}_r]_{(i,j)})^2 + \mu\sum_{r=1}^{R}\|\boldsymbol{S}_r\|_*. \quad (11)$$

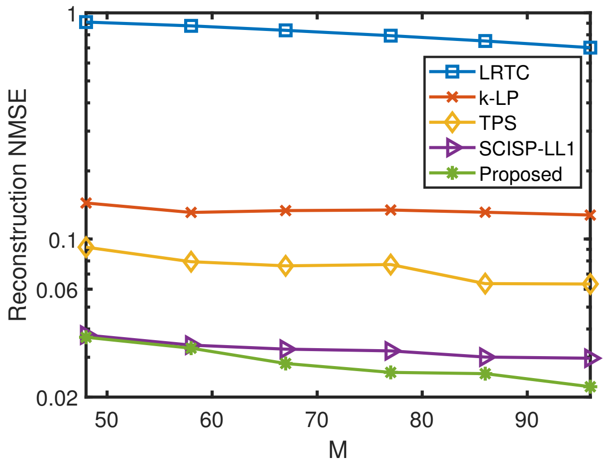

Fig. 1. Reconstruction NMSE versus M

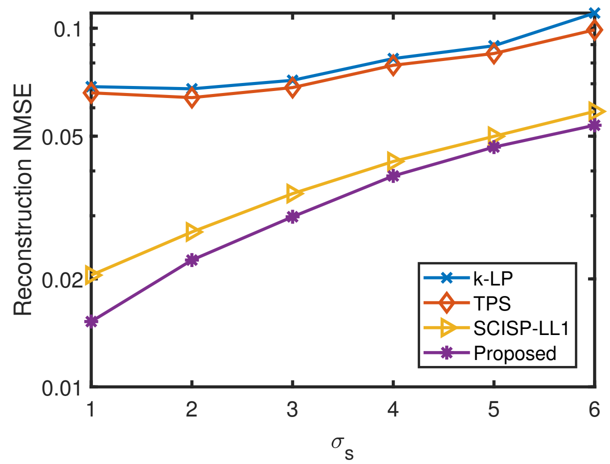

Fig. 2. Reconstruction NMSE versus σ_s

Based on the low-rank property, we assume the rank $0 \leq l \leq \min(N_1, N_2)$ of $\boldsymbol{S}_r$. Then, using the singular value thresholding algorithm, the solution is $\hat{\boldsymbol{S}}_r = \boldsymbol{U}_l \boldsymbol{\mathcal{S}}_\mu(\boldsymbol{\Sigma}_l)\boldsymbol{V}_l^{\mathrm{T}}$ where the soft-thresholding operator $\boldsymbol{\mathcal{S}}_\mu(\boldsymbol{\Sigma}) = \mathrm{diag}[(\sigma_1-\mu)_+, \cdots (\sigma_l-\mu)_+]$, $(x)_+ = \max(0, x)$, σ_l represents singular value, and $\boldsymbol{\Psi} = \boldsymbol{U}_l\boldsymbol{\Sigma}_l\boldsymbol{V}_l^{\mathrm{T}}$ where $\boldsymbol{\Psi}$ is constructed based on $\boldsymbol{e}_r^{\mathrm{T}}\boldsymbol{\theta}_{ij}$.

The alternating regression and singular value thresholding algorithm holds convergence property [20]. Finally, we can obtain the power spectrum from $\hat{\boldsymbol{\mathcal{H}}} = \sum_{r=1}^{R} \hat{\boldsymbol{S}}_r \circ \hat{\boldsymbol{\phi}}^{(r)}$.

4. NUMERICAL RESULTS

We adopt model (3) to simulate the power spectrum map in an $L \times L$ area for $L = 300$ meters, where $g_r(d) = P_r(C_0/d)^2$ follows Friis transmission equation, $d = \sqrt{x^2 + y^2}$ represents the distance from the source, (x, y) is the coordinate. We choose the parameter $P_r = 1\mathrm{W}$, $C_0 = 2$ for illustrative purpose. Other values are broadly similar. The power spectrum $\phi_k^{(r)}$ is generated by $\phi_k^{(r)} = \sum_{i=1}^{2} a_i^{(r)} \mathrm{sinc}^2(k - f_i^{(r)}/b_i^{(r)})$, where $a_i^{(r)} \sim \mathcal{U}(0.5, 2)$, $f_i^{(r)} \in \{1, \cdots, K\}$ is the center of the i-th square sinc function, $b_i^{(r)} \sim \mathcal{U}(2, 4)$ and $K = 20$. The sensors are distributed uniformly at random in the area to collect the signal power $\gamma_m^{(k)}$. The shadowing component in log-scale $\log_{10}\zeta$ is modeled using a Gaussian process with zero mean and auto-correlation function $\mathbb{E}\{\log_{10}\zeta(\boldsymbol{z}_i)\log_{10}\zeta(\boldsymbol{z}_j)\} = \sigma_{\mathrm{s}}^2\exp(-||\boldsymbol{z}_i - \boldsymbol{z}_j||_2/d_{\mathrm{c}})$, in which correlation distance $d_{\mathrm{c}} = 30$ meters, shadowing variance $\sigma_s = 1$. The $\tilde{\epsilon}$ follows Gaussian distribution $\mathcal{N}(0, \sigma^2)$, we choose $\sigma = 1$.

We employ the normalized mean squared error (NMSE) of the reconstructed power spectrum map for performance evaluation. Let $\mathrm{NMSE} = ||\hat{\boldsymbol{\mathcal{H}}} - \boldsymbol{\mathcal{H}}||_F^2/||\boldsymbol{\mathcal{H}}||_F^2$. The performance is compared with the following baselines that are recently developed or adopted in related literature. Baseline 1: Thin plate spline (TPS) [21]. Baseline 2: k-nearest neighbor local polynomial interpolation (k-LP) [22]. Baseline 3: low-rank tensor completion (LRTC) [23]. Baseline 4: SCISP-LL1 [17], we first perform TPS, then, the uncertainty is derived and imposed as the restriction on the BTD method.

We quantify the power spectrum map reconstruction performance of the proposed schemes under different number of measurements M = 43–96 of sampling rate 5%–10% with fixed resolution $N = 31$ and number of sources $R = 2$. Fig. 1 shows that that the proposed method outperforms the baseline methods with more than 10% improvement in the reconstruction accuracy when the sampling rate is larger than 6%. The worse performance of low-rank tensor completion is due to the off-grid sparse observations. The worse performance of TPS and k-LP is due to the lack of the ability to exploit the correlation property in the spectral domain. The SCISP-LL1 is similar to the proposed method when the sampling rate is 5%–6%, but the performance increases slowly with M increase. Because it does not exploit the correlation property when using the TPS interpolation.

We also quantify the reconstruction performance of the proposed schemes under different shadowing variance σ_s = 1–6 under sampling rate 10%. Fig. 2 demonstrates the performance of the proposed method outperforms the baseline methods with more than 8% improvement under the shadowing variance σ_s = 1–6.

5. CONCLUSION

In this paper, we propose an off-grid tensor-guided interpolation. We use a segmented polynomial model to handle the off-grid measurements and the nuclear norm regularization to capture the low-rank property of each source. Then, we develop an alternating minimization algorithm. The numerical results show the superiority of the proposed method.

6. REFERENCES

[1] H. Sun and J. Chen, "Grid optimization for matrix-based source localization under inhomogeneous sensor topology," in *Proc. IEEE Int. Conf. Acoustics, Speech, and Signal Processing*, 2021, pp. 5110–5114.

[2] J. Gao, D. Wu, F. Yin, Q. Kong, L. Xu, and S. Cui, "Metaloc: Learning to learn wireless localization," *IEEE J. Sel. Areas Commun.*, vol. 41, no. 12, pp. 3831–3847, 2023.

[3] J. Gao, C. Zhang, Q. Kong, F. Yin, L. Xu, and K. Niu, "Metaloc: Learning to learn indoor rss fingerprinting localization over multiple scenarios," in *Proc. IEEE Int. Conf. Commun.*, 2022, pp. 3232–3237.

[4] X. Mo, Y. Huang, and J. Xu, "Radio-map-based robust positioning optimization for uav-enabled wireless power transfer," *IEEE Wireless Commun. Lett.*, vol. 9, no. 2, pp. 179–183, 2019.

[5] F. Shen, Z. Wang, G. Ding, K. Li, and Q. Wu, "3d compressed spectrum mapping with sampling locations optimization in spectrum-heterogeneous environment," *IEEE Trans. on Wireless Commun.*, vol. 21, no. 1, pp. 326–338, 2022.

[6] K. Sato, K. Suto, K. Inage, K. Adachi, and T. Fujii, "Space-frequency-interpolated radio map," *IEEE Trans. Veh. Technol.*, vol. 70, no. 1, pp. 714–725, 2021.

[7] Y. Zhang and S. Wang, "K-nearest neighbors gaussian process regression for urban radio map reconstruction," *IEEE Commun. Lett.*, vol. 26, no. 12, pp. 3049–3053, 2022.

[8] M. Hamid and B. Beferull-Lozano, "Non-parametric spectrum cartography using adaptive radial basis functions," in *Proc. IEEE Int. Conf. Acoustics, Speech, and Signal Processing*, 2017, pp. 3599–3603.

[9] S.-J. Kim and G. B. Giannakis, "Cognitive radio spectrum prediction using dictionary learning," in *Proc. IEEE Global Telecomm. Conf.*, 2013, pp. 3206–3211.

[10] S. G. Sathyanarayana, Z. Wang, N. Sun, B. Ning, S. Hu, and J. A. Hossack, "Recovery of blood flow from undersampled photoacoustic microscopy data using sparse modeling," *IEEE Trans. Med. Imag.*, vol. 41, no. 1, pp. 103–120, 2022.

[11] M. D. Migliore, "A compressed sensing approach for array diagnosis from a small set of near-field measurements," *IEEE Trans. Antennas Propag.*, vol. 59, no. 6, pp. 2127–2133, 2011.

[12] H. Sun and J. Chen, "Regression assisted matrix completion for reconstructing a propagation field with application to source localization," in *Proc. IEEE Int. Conf. Acoustics, Speech, and Signal Processing*, Singapore, May 2022, pp. 3353–3357.

[13] Y. Teganya and D. Romero, "Deep completion autoencoders for radio map estimation," *IEEE Trans. on Wireless Commun.*, 2021.

[14] S. Shrestha, X. Fu, and M. Hong, "Deep spectrum cartography: Completing radio map tensors using learned neural models," *IEEE Trans. Signal Process.*, vol. 70, pp. 1170–1184, 2022.

[15] D. Schaufele, R. L. G. Cavalcante, and S. Stanczak, "Tensor completion for radio map reconstruction using low rank and smoothness," in *Proc. IEEE Int. Workshop Signal Process. Adv. Wireless Commun.*, 2019, pp. 1–5.

[16] G. Zhang, X. Fu, J. Wang, X.-L. Zhao, and M. Hong, "Spectrum cartography via coupled block-term tensor decomposition," *IEEE Trans. Signal Process.*, vol. 68, pp. 3660–3675, 2020.

[17] X. Chen, J. Wang, G. Zhang, and Q. Peng, "Tensor-based parametric spectrum cartography from irregular off-grid samplings," *IEEE Signal Process. Lett.*, vol. 30, pp. 513–517, 2023.

[18] H. Sun and J. Chen, "Propagation map reconstruction via interpolation assisted matrix completion," *IEEE Trans. Signal Process.*, vol. 70, pp. 6154–6169, 2022.

[19] J. Fan, *Local polynomial modelling and its applications: Monographs on statistics and applied probability 66*. Routledge, 1996.

[20] D. P. Bertsekas, "Nonlinear programming," *Journal of the Operational Research Society*, vol. 48, no. 3, pp. 334–334, 1997.

[21] J. A. Bazerque, G. Mateos, and G. B. Giannakis, "Group-lasso on splines for spectrum cartography," *IEEE Trans. Signal Process.*, vol. 59, no. 10, pp. 4648–4663, 2011.

[22] A. Verdin, C. Funk, B. Rajagopalan, and W. Kleiber, "Kriging and local polynomial methods for blending satellite-derived and gauge precipitation estimates to support hydrologic early warning systems," *IEEE Trans. Geosci. Remote Sens.*, vol. 54, no. 5, pp. 2552–2562, 2016.

[23] J. Liu, P. Musialski, P. Wonka, and J. Ye, "Tensor completion for estimating missing values in visual data," *IEEE Trans. Pattern Anal. Mach. Intell.*, vol. 35, no. 1, pp. 208–220, 2013.